Int. J. Electrochem. Sci., 15 **(2020)** 9707 – 9719, doi: 10.20964/2020.10.56

International Journal of ELECTROCHEMICAL SCIENCE
www.electrochemsci.org

Corrosion Resistance of the UNS N26455 Superalloy in Simulated Environment Containing Chloride and CO_2

José Henrique Alano[1,], Renato Luiz Siqueira, Régis Djiovanni da Cruz Rosca[1], Amanda Dantas de Oliveira[2], Guilherme dos Santos Vacchi[3], Sebastião Elias Kuri[3], Ricardo Marques e Silva[3,*], Carlos Alberto Della Rovere[3,*]*

[1] Escola de Engenharia, Universidade Federal do Rio Grande, Campus Carreiros, 96203-900, Rio Grande, RS, Brazil
[2] Centro de Desenvolvimento Tecnológico, Universidade Federal de Pelotas, Rua Gomes Carneiro 1, 96010-610, Pelotas, RS, Brazil
[3] Universidade Federal de São Carlos, Programa de Pós-Graduação em Ciência e Engenharia de Materiais, Rodovia Washington Luís km 235, 13565-905, São Carlos, SP, Brazil
[*]E-mail: henrique.al@gmail.com; ricardomarqueseng@gmail.com; rovere@ufscar.br

Received: 4 June 2020 / *Accepted:* 30 July 2020 / *Published:* 31 August 2020

UNS N26455 is a superalloy commonly used on offshore platforms in components for injection pumps due to its appreciable resistance to various forms of corrosion. However, this superalloy sustain damage under aggressive operating conditions, such as in the presence of chloride ions (Cl^-), harmful gases or even thermal variations. Hence, the corrosion resistance of UNS N26455 was evaluated via the anodic potentiodynamic polarization technique to understand its behavior under potentially harmful working conditions. The experiments were carried out in controlled environments containing high Cl^- concentrations at different temperatures (25 and 40 °C), with and without carbon dioxide (CO_2) saturation. The results confirmed that the as-cast superalloy is highly resistant to localized corrosion. On the other hand, the influence of the formation of its microstructure's secondary phase, which occurs when it is exposed to high temperatures for a prolonged period of time, still needs to be investigated properly.

Keywords: nickel superalloy, corrosion resistance, anodic polarization.

1. INTRODUCTION

Nickel (Ni)-based superalloys are solid solutions formed from the combination of Ni with other chemical elements. They are often used in applications that require great mechanical strength and structural stability at medium and high temperatures [1–3]. Corrosion resistance is also an important requirement for this class of materials, increasing its useful life as well as making it suitable for other applications. Iron (Fe)-based stainless steel is one material that can be replaced by Ni-based superalloys

because, although the Fe-based materials are cheaper, they have lower corrosion resistance. Such a substitution makes sense in the case of components used in offshore oil platforms because they are exposed to high Cl^- concentrations in the presence of corrosive gases and must function under variations in temperature. These conditions are severe in terms of corrosion and therefore require materials with high resistance to different forms of corrosion, such as pitting or the formation of crevices [4].

Ni-based superalloys typically have an austenitic matrix γ (gamma phase) with a face-centered cubic structure (FCC) that provides high tensile strength and protection against rupture, as well as adequate creep properties [1–3]. Their stability ensures excellent performances at high temperatures during thermal cycles and over long periods of operation. Moreover, the austenitic matrix supports the solubility of several elements in considerable amounts, making it possible to produce an extensive variety of alloys [1–3]. For example, chromium (Cr), molybdenum (Mo), and tungsten (W) can be added to alloys in order to achieve the best set of properties for certain applications. However, such elements must be used carefully because, depending upon their exposure times to high temperatures, they can promote the formation of topologically close-packed (TCP) phases [2, 4, 5], which will modify the expected properties of the materials.

Of the superalloys in the Ni–Cr–Mo system, it is important to highlight those materials with between 15 and 22 wt% Cr, which belong to the group known as the C-alloys. They exhibit high corrosion resistance in both oxidizing and reducing environments [6, 7], a property which makes these materials suitable for use in several industrial sectors where distinctive corrosive environments are found. A well-studied material in this group is the UNS N06022 superalloy (Ni–22Cr–13Mo–3Fe–3W) [6–10], which has good corrosion resistance in oxidizing (effect of Cr) and reducing (effects of Mo and W) environments. This characteristic makes the UNS N06022 superalloy advantageous in applications where mixed acids are present and makes it a potential engineering barrier for geological repositories designed to contain nuclear waste [11]. Another material from this group, the UNS N26455 (Ni–16Cr–16Mo) superalloy, which is evaluated in this study, is used in parts for injection pumps for offshore platforms, among other uses. Although the C-alloys are known for their remarkable corrosion resistance, the susceptibility of an individual alloy depends strongly on its composition, microstructure, and working environment. Thus, the purpose of this study was to investigate the influence of environments containing high Cl^- at different temperatures, with or without CO_2 saturation, on the corrosion resistance of the UNS N26455 superalloy. Severe environments were carefully selected to simulate (and extrapolate) possible service conditions.

2. MATERIALS AND METHODS

2.1. Preparations of samples and characterization

The UNS N26455 superalloy was provided by *Sulzer Brazil S.A.* The cast material was received in cylindrical bars of dimension 200 x 25 mm ($L\ x\ \emptyset\ mm$). Table 1 shows the chemical composition of the as-received superalloy in comparison with the specifications in ASTM A494/A494M-18a [12].

Table 1. Chemical composition (wt%) of the UNS N2645 superalloy and its ASTM specification.

UNS N26455	C	Cr	Ni	Mn	Si	Mo	S	P
As-received	0.027	16.75	64.75	0.81	0.55	17.10	0.0089	0.0038
ASTM A494	0.02_{max}	15-17.5	balance	1.0_{max}	0.8_{max}	15-17.5	0.03_{max}	0.03_{max}

The crystalline phase was identified by X-ray diffraction (XRD) using a Bruker D8 ADVANCE diffractometer operated with CuKα radiation (λ = 0.15418 nm). The diffractogram was acquired in the range of 2θ from 30 to 110° in continuous mode at 1°/min. A microstructural analysis was performed following the ASTM E3-11(2017) [13]. Samples in as-cast condition and after a heat treatment at 750 °C for 360 h (in air) were sanded progressively with 240-, 400-, 600-, and 1200-grit silicon carbide (SiC) sandpapers. Afterward, they were polished with 0.3 µm alumina paste and cleaned with distilled water and isopropanol. Finally, the samples were immersed in *aqua regia* (HNO_3 : 3HCl ratio) for 90 s to reveal their microstructures, and then were analyzed via scanning electron microscopy (SEM) using a Phillips FEG X-L30 microscope coupled with an energy dispersive X-ray spectrometer (EDS), which allowed for qualitative chemical analysis.

2.2. Electrochemical assay

The potentiodynamic anodic polarization technique was used to assess the corrosion resistance of the UNS N26455 superalloy following ASTM G5–94(2011)e1 [14]. A potentiostat Gamry Reference 3000 was used to conduct the electrochemical experiment, and the acquired data were analyzed using DC105™ DC Corrosion software. The conventional electrochemical cell used was composed of a counter electrode of platinum (Pt), a reference electrode of saturated calomel (SCE), and a 10 x 5.1 mm (L x Ø mm) cylindrical working electrode created from the samples using electro-erosion. For each working electrode, a copper wire (AWG 35) was welded onto one face to make electrical contact, and the system was insulated with polyester resin while leaving the other face exposed to the environment for analysis, as shown in Figure 1. Before measurements were taken, this exposed area on each working electrode was sanded sequentially with 240-, 400-, 600-, and 1200-grit SiC sandpapers and cleaned with distilled water prior to immersed in the electrochemical cell.

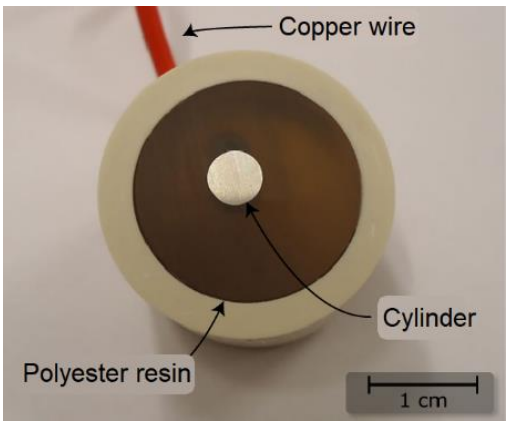

Figure 1. Working electrode prepared for a potentiodynamic anodic polarization assay.

Different combinations of Cl^- concentration, CO_2 saturation, and temperature were evaluated, as shown in Table 2. Solutions containing 2.82 and 5.08 mol/L Cl^- were prepared from sodium chloride (NaCl) that had concentrations approximately 5 and 9 times higher than that of seawater, respectively [15]. The assays were carried out in naturally aerated chloride solutions, with or without CO_2 saturation, at 25 and 40 °C. A water-cooled condenser was coupled to the electrochemical cell to avoid possible variations in the electrolyte concentration at both temperatures. In the assays with CO_2 saturation, CO_2 gas (80 mL/min) flowed through the electrolyte for 40 min. This time was established in advance by monitoring the pH of the medium until a constant value of 3.5 was reached. For each electrochemical assay, at least three measurement were recorded, and all values presented are the average results.

Table 2. Conditions under which the potentiodynamic anodic polarization assays took place.

Experiment	Cl^- concentration (mol/L)	Temperature (°C)	CO_2 saturation
1	2.82	25	Unsaturated
2	2.82	25	Saturated
3	2.82	40	Unsaturated
4	2.82	40	Saturated
5	5.08	25	Unsaturated
6	5.08	25	Saturated
7	5.08	40	Unsaturated
8	5.08	40	Saturated

Initially, the working electrodes were exposed to the simulated environments until they reached a steady state defined as the open circuit potential (E_{OC}). Subsequently, the corrosion potential (E_{corr}) for each combination was defined as the mean of at least three E_{OC} values for that set of conditions. Then, for each combination, a potential scan was conducted at a rate of 1 mV/s in the anodic direction from 200 mV below the E_{OC} up to 1000 mV_{SCE} in order to obtain the desired electrochemical parameters.

3. RESULTS AND DISCUSSION

3.1. Characterization of the superalloy

Figure 2 shows the X-ray diffractogram of the as-cast UNS26455 superalloy after it was treated at 750 ºC for 360 h, making it possible to observe only the peaks related to the austenitic γ phase. The intense peak centered at 43.66° (2θ) and the other less-intense peaks at 50.64, 74.46, and 90.41° (2θ) correspond to the (111), (200), (220), and (311) atomic planes in the γ lattice, respectively. This austenitic phase is composed of a solid solution formed between Ni and the other elements contained in the superalloy composition, as specified in Table 1.

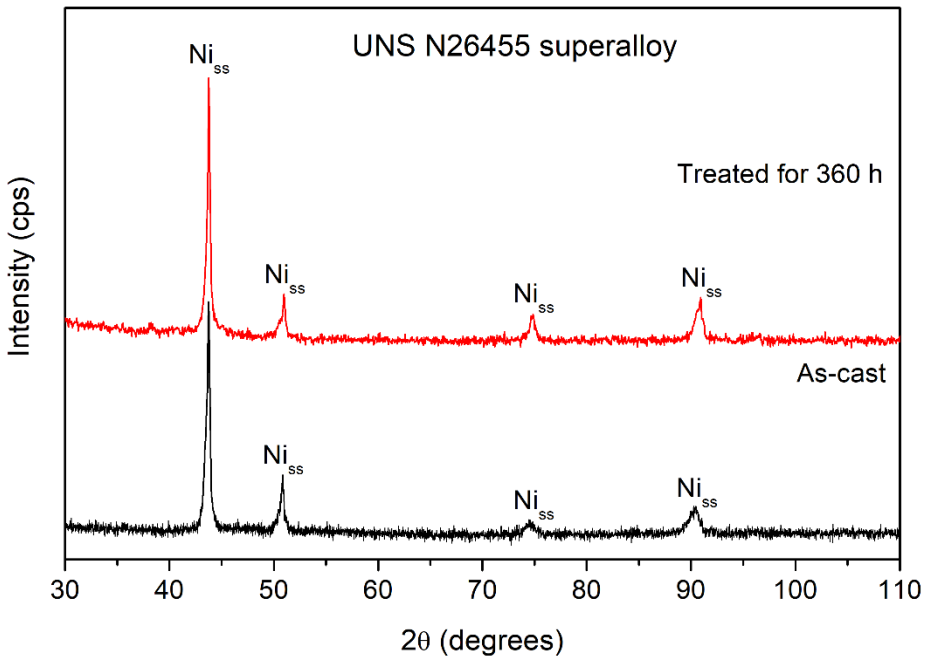

Figure 2. X-ray diffractograms of the UNS N26455 superalloy: Ni_{ss} = nickel solid solution.

Only the γ phase was identified in the X-ray diffractograms, but the SEM micrographs in Figure 3 revealed the presence of a secondary phase (bright precipitates) in both the as-cast and treated samples owing to the contrast generated by differences in their chemical compositions compared to the matrices (dark phase). Even after increasing the concentration with the heat treatment, the XRD technique was unable to make an accurate identification of this secondary phase. The formation of this secondary phase may be associated with the segregation of some components of the matrix during the casting of the superalloy, a process that involves high temperatures. Some pores were also observed inherent to this manufacturing process.

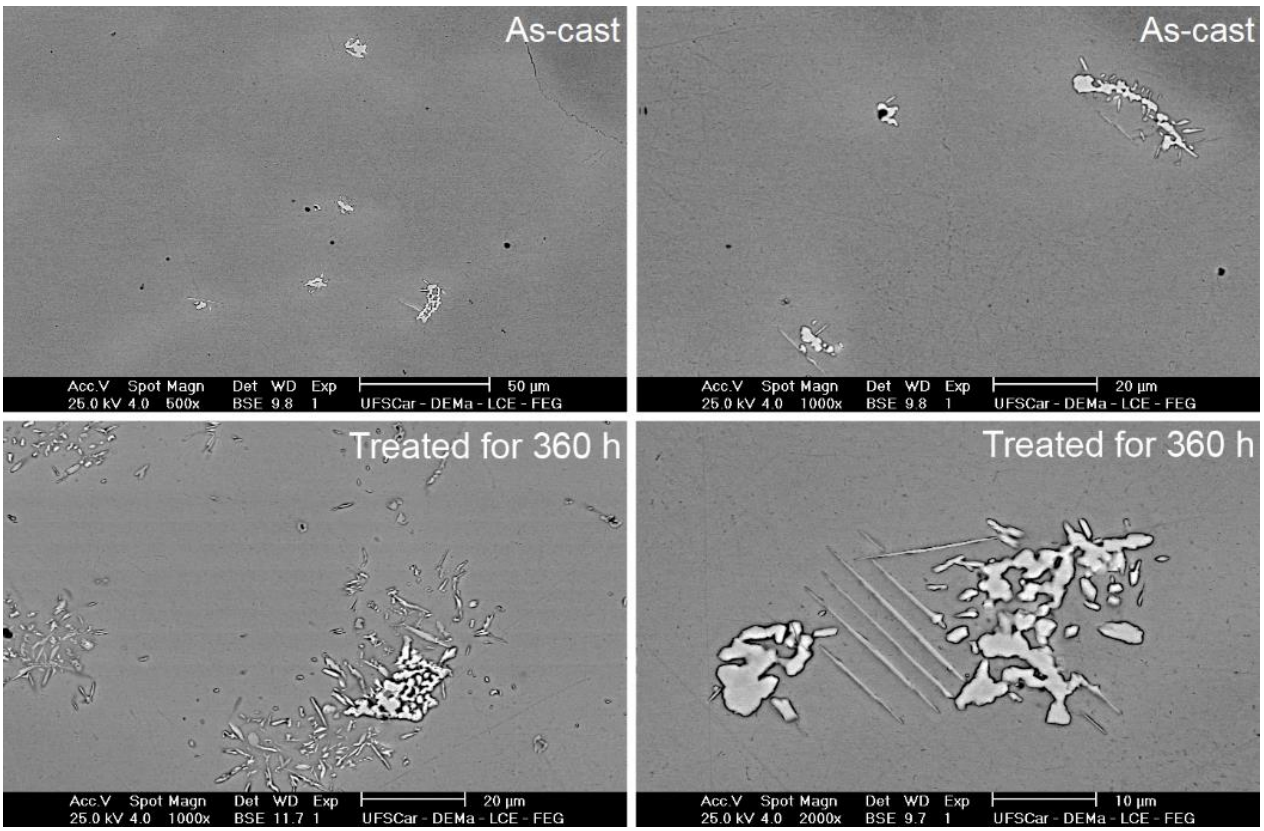

Figure 3. SEM micrographs of the as-cast UNS26455 superalloy and the same superalloy after heat treatment at 750 °C for 360 h following immersion in *aqua regia*.

Table 3 displays the separate EDS analyses for the major chemical elements present in the superalloy (overview), precipitates, and matrix. The Ni, Cr, and Mo concentrations in the superalloy are consistent with those shown in Table 1. The precipitates also contain Ni and Cr, but they are rich in Mo, indicating the formation of the intermetallic P phase, roughly presenting the $Cr_{18}Mo_{42}Ni_{40}$ stoichiometry. This phase is often identified in Ni–Cr–Mo alloys [2, 5, 11], and its composition can vary, as can the compositions of several other TCP phases.

Table 3. EDS results for the Ni, Cr, and Mo concentrations (wt%) in the superalloy, precipitate, and matrix. The missing percentages of chemical elements correspond to minority elements.

Analysis area	Ni	Cr	Mo
Superalloy (overview)	65.86	16.20	16.09
Precipitate	40.18	10.90	44.69
γ matrix	69.07	16.47	13.06

The elemental maps in Figure 4 shows the migration of these elements (mainly Mo) in the formation of the new phase, causing specific and significant changes in the matrix composition. TCP phases with large amounts of Cr and Mo result in the depletion of these elements in regions adjacent to the precipitates, a condition which may facilitate the development of localized corrosion [16, 17].

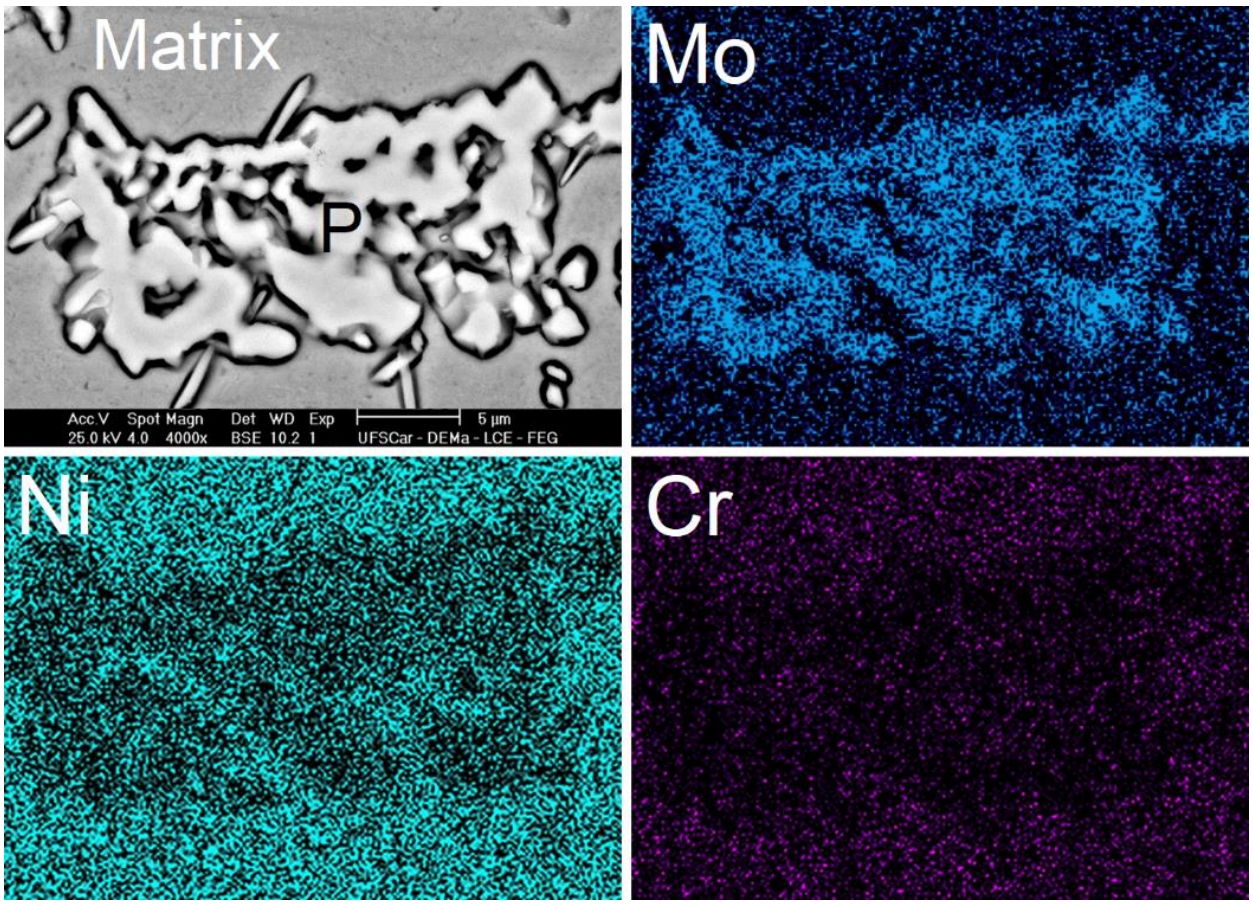

Figure 4. SEM micrograph of a precipitate following immersion in *aqua regia*, and the elemental maps showing the distributions of Mo, Ni, and Cr.

In general, the addition of Cr to Ni-based alloys improves corrosion resistance by providing the spontaneous formation of a protective oxide film composed essentially of Cr_2O_3. On the other hand, Mo improves the alloy's repassivation behavior and consequently its resistance to localized corrosion by blocking the growth of pits and inhibiting the diffusion of species into or out of these pits [18–20]. Therefore, the reductions in Cr and Mo in the matrix due to the formation of the secondary phase may affect, in some way, the material's resistance to localized corrosion.

The addition of some elements to the superalloy and their respective concentrations can lead to the formation of TCP phases (rich in these elements), as mentioned above. These intermetallic phases usually have high densities of packed atoms and complex crystalline structures. With respect to the P phase, it is orthorhombic and contains 56 atoms per unit cell [2] being possible to predict its precipitation using a Ni–Cr–Mo diagram [21], which has a stability field that increases with increasing temperature. For example, in a 55.7Ni–21.1Cr–13.5Mo alloy, increasing the treatment time can result in higher amounts of P phase, and the P phase's growth kinetics are considerable at temperatures close to 750 °C [22]. So, conducting a heat treatment, it was also possible to verify an increase in the amount of secondary phase in the UNS26455 superalloy when it was exposed to 750 °C for 360 h, as demonstrated in Figure 3. ImageJ® software was used to estimate the amounts of secondary phase in the as-cast (0.25%) and treated (3.5%) samples. This significant increase in the secondary phase in the alloy's microstructure is in good

agreement with the time-temperature-transformation diagram (TTT) described by Turchi and co-authors [22]. This diagram suggests that ~8% of the material will be in the P phase when the alloy is assayed for 1000 h in a thermal aging treatment. Therefore, the amount of P phase in the UNS N26455 superalloy may vary according to the time the alloy is exposed to high temperatures. As this intermetallic phase formation reduces the alloying elements contained in the matrix (particularly Mo), its concentration can also play an essential role in the development of localized corrosion in the alloy.

3.2. Corrosion resistance

The corrosion resistance of the UNS N26455 superalloy was evaluated under eight different conditions, as shown in Table 2. The potentiodynamic polarization curves in Figure 5 show that its anodic behavior has a poorly defined passive region but also that it has the characteristics common to other superalloys in solutions containing chloride ions [23]. A marked increase in current density (I_A) at potentials above 700 mV_{SCE} was verified for all tested combinations. The increase in I_A at high potential values could be attributed to the water decomposition reaction (E_{wd}), $2H_2O \rightarrow O^{2+} + 4H^+ + 4e^-$ [20], presence of pits [23] or transpassive dissolution of the oxide film (E_{td}) [24]. Metals and alloys with passive behavior commonly have widespread corrosion resistance, making them more susceptible to localized corrosion, such as the formation of pits and crevices [25]. Localized corrosion occurs when the passive film is broken at specific locations on the metal's surface, resulting in fast and localized attacks [25–27]. In an anodic polarization curve, a break in the passive film is expressed as a sharp increase in the I_A. When such an increase occurs at lower (more active) potentials, it can be explained by the stabilization of localized corrosion. This potential is known as the pitting potential (E_{pit}) in the case of pitting corrosion or the breakdown potential (E_b) in the case of crevice corrosion. Transpassive dissolution is also marked by an increase in I_A, but this increase typically occurs at higher potentials [28].

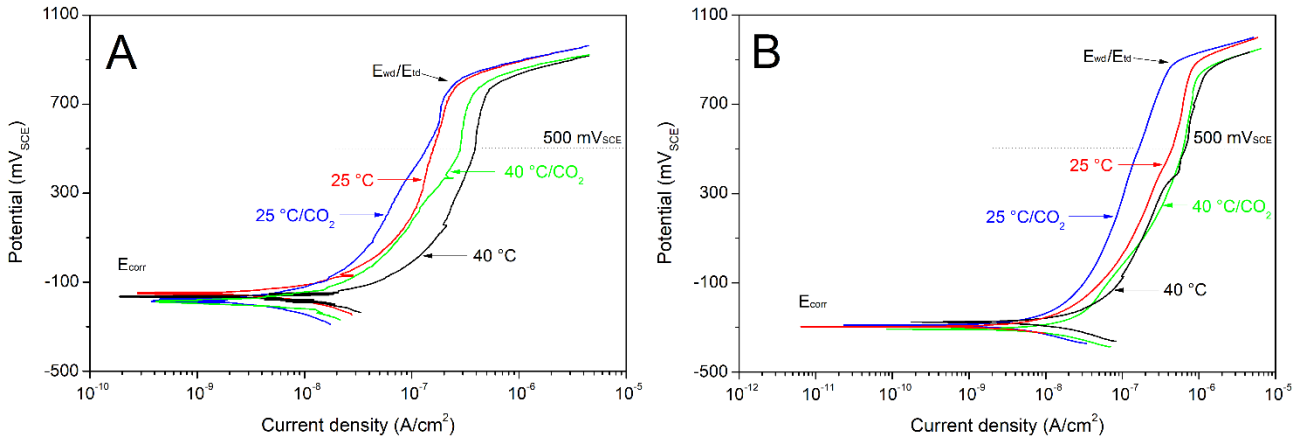

Figure 5. Potentiodynamic anodic polarization curves of the UNS N26455 superalloy in NaCl solution, with and without CO_2 saturation, at 25 and 40 ºC: A) 2.82 mol/L Cl^- and B) 5.08 mol/L Cl^-.

The potentiodynamic anodic polarization assay performed in a solution containing 5.08 mol/L Cl^- at 40 °C, one of the most aggressive combinations, produced no pitting corrosion, as shown in Figure

6. Hence, the increase in the I_A may be attributed to the E_{wd} or E_{td} on the working electrode surface. According to the Nernest equation, $E_{O/H+}$ (V_{SCE}) = 0.978 – 0.059 pH [29], thus, the oxygen reduction reaction should have occurred at approximately 630 mV_{SCE} without CO_2 saturation (pH = 5.9) and close to 770 mV_{SCE} for the solution saturated in CO_2 (pH = 3.5). These potentials are close to the values obtained experimentally, indicating the influence of this reaction in the abrupt increase in the I_A. Moreover, increasing the Cl^- concentration did not reduce the value of the breaking potential, which is to be expected when the increase in current comes from the development of pitting corrosion.

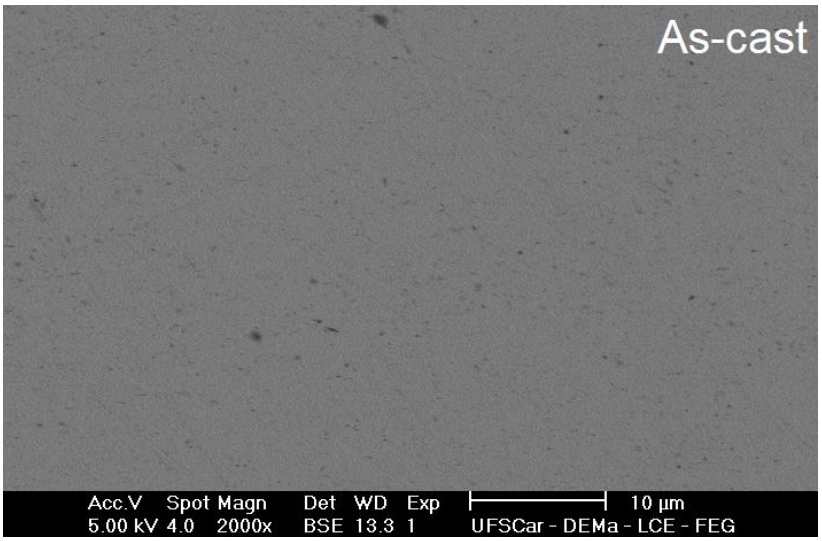

Figure 6. SEM micrograph of the as-cast UNS N26455 superalloy after its potentiodynamic anodic polarization assay in NaCl solution containing 5.08 mol/L Cl^- at 40 ºC.

The E_{corr} values decreased with increasing Cl^- concentration. The lower E_{corr} values, together with the increase in I_A, indicate a reduction in the corrosion resistance of the material [30, 31]. The effect of Cl^- on the areas with imperfections in the passive film exposing the most active areas on the electrode reduced the E_{corr} values [32]. Although the E_{corr} values changed with changes in the Cl^- concentration, the CO_2 saturation and variation in temperature did not have significant influences, as demonstrated in Table 4. The E_{wd}/E_{td} potentials exhibited slight, but significant, changes, which were mainly evident with the increase in the Cl^- concentration. The I_A at 500 mV_{SCE}, which was defined arbitrarily for comparison purposes, changed with increasing temperature and CO_2 saturation. It shifted to higher values but remained within the same order of magnitude. Therefore, we found that the UNS N26455 superalloy has outstanding corrosion resistance under the combinations used in all experiments.

Table 4. The E_{corr}, E_{wd}/E_{td}, and I_A results for the assays carried out for the various combinations at 500 mV_{SCE}.

Experiment	E_{corr} (mV_{SCE})	E_{wd}/E_{td} (mV_{SCE})	I_A (A/cm^2)
1	-124	776	1.37×10^{-7}
2	-167	781	1.58×10^{-7}
3	-143	760	1.37×10^{-7}
4	-154	778	1.58×10^{-7}
5	-293	874	1.67×10^{-7}
6	-273	868	4.44×10^{-7}
7	-255	832	6.20×10^{-7}
8	-259	839	6.61×10^{-7}

Figure 7 shows the potentiodynamic anodic polarization curves comparing the as-cast UNS N26455 superalloy and the same superalloy after heat treatment, when it contained a higher amount of P phase. The assay was performed under the most aggressive proposed conditions, i.e., with CO_2 saturation and 5.08 mol/L Cl^- at 40 °C. An increase in the passive current density is observed when the potential reaches approximately 250 mV_{SCE} and as it progresses up to 450 mV_{SCE}. Another increase occurs when the potential reaches ~850 mV_{SCE}. Mishra and Frankel [33] described similar anodic behavior for the UNS N06022 superalloy exposed to 1 M NaCl at 90 ºC, and these authors attributed the first increase in I_A to the formation of crevices and the second to E_{td}. In Figure 7, a transition in active/passive behavior in potentials above 450 mV_{SCE} is also observed, suggesting that after the selective dissolution of superficial precipitates, the exposed electrode areas consisted exclusively of the austenitic matrix. Thus, the current density tended to decrease due to the repassivation of these dissolved regions.

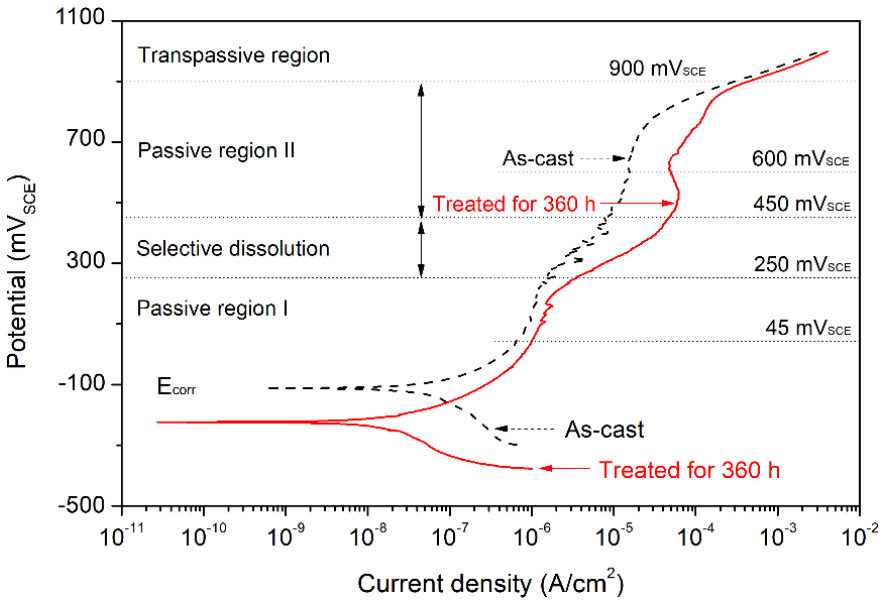

Figure 7. Potentiodynamic anodic polarization curves of the as-cast UNS N26455 superalloy and the same superalloy after heat treatment at 750 °C for 360 h. The assay was performed in NaCl solution containing 5.08 mol/L Cl^- and with CO_2 saturation at 40 °C.

With the heat treatment and growth of the secondary phase, the superalloy presented two passive regions separated a selective dissolution region, then a transpassive region at around 900 mV_{SCE}. A decrease in the mean E_{corr} value from -199.06 mV_{SCE} to -224.10 mV_{SCE} was also observed and associated with the amount of P phase because the Cl^- concentration was the same in these assays. Decreases in the E_{corr} can be obtained by favoring anodic or restricting cathodic processes on the electrode surface [34]. Thus, the amount of P phase can increase the anodic reaction rate on the electrode surface, justifying the reduction in the E_{corr}. The decrease in the E_{corr} can also be supported by the Point Defect Model (PDM) [26], which says that the growth of a passive film is proceeded by reactions at the metal/film and film/solution interfaces when cation vacancies are the predominant punctual defects in *p*-type films or oxygen vacancies and/or interstitial cations are the predominant defects in *n*-type films. Hence, it is possible that the increase in the amount of P phase has changed the concentration of the donors or acceptors in the passive film and nudged the E_{corr} towards more active potential values. Of course, more in-depth studies are needed to explain the differences observed in E_{corr} in detail.

In the first passive region, the I_A value, defined at 45 mV_{SCE}, increases from 6.61 x 10^{-7} to 1.00 x 10^{-6} A/cm^2 in a comparison of the as-cast and heat-treated samples. In the second passive region, with the potential at 600 mV_{SCE}, the anodic behavior of the superalloy was similar, and the I_A value changed from 1.58 x 10^{-5} to 5.00 x 10^{-5} A/cm^2. These data indicate the selective dissolution of the P phase, in which its higher concentration corresponded to the greater dissolution current. The SEM micrographs of the heat-treated sample after the potentiodynamic anodic polarization assay are shown in Figure 8, confirming the dissolution of the secondary P phase. The only attacks present in the superalloy occurred in the areas where the precipitates had grown, while no localized corrosion was found in the austenitic matrix.

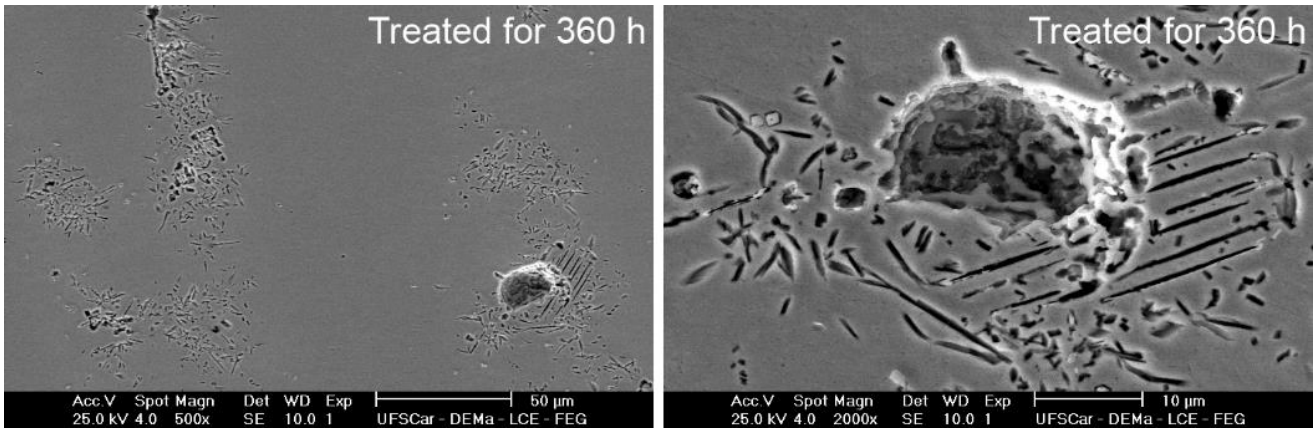

Figure 8. SEM micrographs of the UNS N26455 superalloy treated at 750 °C for 360 h after the potentiodynamic anodic polarization assay performed in NaCl solution containing 5.08 mol/L Cl^- and CO_2 saturation at 40 °C.

Thus, the exposure of this superalloy at high temperatures benefits the precipitation of the intermetallic P phase that can favor localized corrosion. This event may contribute to the reduction of the useful life of the material and its failure in service. For this reason, further investigations into the secondary phase effect on the corrosion resistance of the UNS N26455 superalloy are necessary.

4. CONCLUSION

The corrosion resistance of the UNS N26455 superalloy was studied via the potentiodynamic anodic polarization technique. Possible service conditions on offshore platforms were simulated, and this superalloy demonstrated outstanding resistance to localized corrosion, even under aggressive conditions containing a high Cl^- concentration and CO_2 saturation at different temperatures. However, the amount of P phase in the microstructure affected its anodic behavior, reducing the E_{corr} and increasing the I_A value significantly in potentials above 200 mV_{SCE} due to its selective dissolution. The precipitate regions were repassivated after the complete P phase dissolution, stabilizing the I_A and defining a second passive region. Therefore, as the presence of the intermetallic P phase in the material's microstructure has a deleterious effect in relation to its corrosion resistance, exposure of the UNS N26455 superalloy to high temperatures should be avoided.

ACKNOWLEDGMENTS
This study was financed in part by the Coordenação de Aperfeiçoamento de Pessoal de Nível Superior - Brasil (CAPES) - Finance Code 001. We thank the Brazilian agency CNPq for the financial support and the LCE (UFSCar) and CEME-SUL (FURG) for the characterization analyses. We also thank Sulzer Brasil S.A. for supplying the superalloy samples.

References

1. M. J. Donachie, S. J. Donachie, *Superalloys: a technical guide*, ASM International, (2002) Materials Park, OH, United States of America.
2. R. Reed. *The superalloys: fundamentals and applications*, Cambridge University Press, (2006) Cambridge, United Kingdom.
3. E.Akca and A. Gursel, *PEN.,* 3 (2015) 15.
4. Z. Szklarska-Smialowska, *Pitting and crevice corrosion*, Nace International, (2005) Houston, TX, United States of America.
5. S.H.M. Anijdan and A. Bahrami, *Mater. Sci. Eng., A* 396 (2005) 138.
6. A.S. Wilson, *Mater. Sci. Technol.*, 33 (2017) 1108.
7. P. Crook, *Adv. Mater. Processes,* 165 (2007) 31.
8. C.A.C. Sequeira, D.S.P. Cardoso, L. Amaral, B. Šljukić and D.M.F. Santos, *Corros. Rev.*, 34 (2016) 187.
9. K.J. Evans, A. Yilmaz, S.D. Day, L.L. Wong, J.C. Estill and R.B. Rebak, *JOM.*, 57 (2005) 56.
10. P. Jakupi, F. Wang, J.J. Noël and D.W. Shoesmith, *Corros. Sci.*, 53 (2011) 1670.
11. S-K. Lee and D.D. Macdonald, *J. Nucl. Mater.*, 503 (2018) 124.
12. R.M. Carranza and M.A. Rodríguez, *Npj Mater. Degrad.*, 1 (2017) 1.
13. ASTM A494 / A494M-18a, *Standard Specification for castings, nickel and nickel alloy*, ASTM International, (2018) West Conshohocken, PA, United States of America.
14. ASTM E3-11(2017), *Standard guide for preparation of metallographic specimens*, ASTM International, (2017) West Conshohocken, PA, United States of America.
15. ASTM G5-94(2011)e1, *Standard reference test method for making potentiostatic and potentiodynamic anodic polarization measurements*, ASTM International, (2011) West Conshohocken, PA, United States of America.
16. T. Pichler, J. Veizer, G. E. M. Hall, *Mar. Chem.*, 64 (1999) 229.
17. D.S. Dunn, Y-M. Pan, K.T. Chiang, L. Yang, G.A. Cragnolino and X. He, *JOM.*, 57 (2005) 49.

18. M.A. Rodríguez, R.M. Carranza and R.B. Rebak, *J. Electrochem. Soc.*, 157 (2010) C1.
19. A.C. Lloyd, J.J. Noël, S. McIntyre and D.W. Shoesmith, *Electrochim. Acta*, 49 (2004) 3015.
20. D.D Macdonald, A. Sun, N. Priyantha and P. Jayaweera, *J. Electroanal. Chem.*, 572 (2004) 421.
21. J.R. Hayes, J.J. Gray, A.W. Szmodis and C.A. Orme, *Corrosion*, 62 (2006) 491.
22. P.E.A. Turchi, L. Kaufman and Z-K. Liu, *Calphad*, 30 (2006) 70.
23. P.E.A. Turchi, L. Kaufman and Z-K. Liu, *Calphad*, 31 (2007) 237.
24. T. Bellezze, G. Roventi and R. Fratesi, *Electrochim. Acta*, 49 (2004) 3005.
25. C.M. Wylie, R.M. Shelton, G.J.P. Fleming and A.J. Davenporta, *Dent. Mater.*, 23 (2007) 714.
26. D.D. Macdonald, *J. Electrochem. Soc.*, 139 (1992) 3434.
27. P. Schmuki, *J. Solid State Electrochem.*, 6 (2002) 145.
28. D.A. Jones, *Principles and prevention of* corrosion, Pearson Education, (1996) New York, United States of America.
29. M.S. Barce, J.H. Alano and S.E. Kuri, Duplex stainless steel and Ni based alloy performance in extremely aggressive environments, In: 7th European Stainless Steel Conference, Como, Italy, 2011.
30. T. Xiang, S. Ding, C. Li, S. Zheng, W. Hu, J. Wang and P. Liu, *Mater. Des.*, 114 (2017) 65.
31. W. Xu, J. Song, J. Sun, Y. Lu and Z. Yu, *ACS Appl. Mater. Interfaces*, 3 (2011) 4404.
32. M-C. Zhao, M. Liu, G-L. Song and A. Atrens, *Corros. Sci.*, 50 (2008) 3168.
33. A.K. Mishra and G.S. Frankel, *Corrosion*, 64 (2008) 836.
34. J. Tang, Y. Shao, J. Guo, T. Zhang, G. Meng and F. Wang, *Corros. Sci.*, 52 (2010) 2050.